Heating efficiency evaluation with mimicking plasma conditions of integrated fast-ignition experiment

Shinsuke Fujioka,[1,*] Tomoyuki Johzaki,[2] Yasunobu Arikawa,[1] Zhe Zhang,[1] Alessio Morace,[1] Takahito Ikenouchi,[1]
Tetsuo Ozaki,[3] Takahiro Nagai,[1] Yuki Abe,[1] Sadaoki Kojima,[1] Shohei Sakata,[1] Hiroaki Inoue,[1] Masaru Utsugi,[1] Shoji Hattori,[1]
Tatsuya Hosoda,[1] Seung Ho Lee,[1] Keisuke Shigemori,[1] Youichiro Hironaka,[1] Atsushi Sunahara,[4] Hitoshi Sakagami,[3]
Kunioki Mima,[1,5] Yasushi Fujimoto,[1] Kohei Yamanoi,[1] Takayoshi Norimatsu,[1] Shigeki Tokita,[1] Yoshiki Nakata,[1]
Junji Kawanaka,[1] Takahisa Jitsuno,[1] Noriaki Miyanaga,[1] Mitsuo Nakai,[1] Hiroaki Nishimura,[1] Hiroyuki Shiraga,[1]
Hideo Nagatomo,[1] and Hiroshi Azechi[1]

[1]*Institute of Laser Engineering, Osaka University, 2-6 Yamada-Oka, Suita, Osaka, 565-0871, Japan*
[2]*Graduate School of Engineering, Hiroshima University, 1-4-1 Kagamiyama, Higashi-Hiroshima, Hiroshima, 739-8527, Japan*
[3]*National Institute for Fusion Science, Toki, Gifu 509-5292, Japan*
[4]*Institute for Laser Technology, 2-6, Yamada-oka, Suita, Osaka, 565-0871, Japan*
[5]*The Graduate School for the Creation of New Photon Industries, 1955-1 Kurematsu, Nishiku, Hamamatsu, Shizuoka, 141-1201, Japan*

A series of experiments were carried out to evaluate the energy-coupling efficiency from heating laser to a fuel core in the fast-ignition scheme of laser-driven inertial confinement fusion. Although the efficiency is determined by a wide variety of complex physics, from intense laser plasma interactions to the properties of high-energy density plasmas and the transport of relativistic electron beams (REB), here we simplify the physics by breaking down the efficiency into three measurable parameters: (i) energy conversion ratio from laser to REB, (ii) probability of collision between the REB and the fusion fuel core, and (iii) fraction of energy deposited in the fuel core from the REB. These three parameters were measured with the newly developed experimental platform designed for mimicking the plasma conditions of a realistic integrated fast-ignition experiment. The experimental results indicate that the high-energy tail of REB must be suppressed to heat the fuel core efficiently.

I. INTRODUCTION

Direct-drive fast-ignition (FI) inertial confinement fusion (ICF) is an alternative approach to ICF, providing potentially high-energy gains with lower driver laser energy and relaxing the requirements on fuel assembly compared to the central hot spot ICF [1,2]. In the FI scheme, a relativistic electron beam (REB) is generated by laser-plasma interactions, the REB travels through the plasma surrounding the compressed fuel core, and a part of the REB deposits their energy in the core. More than 10% of heating efficiency ($\eta_{\rm heat}$) is required to achieve the goal of FIREX project [3] with 10 kJ-PW laser LFEX [4]. The heating efficiency ($\eta_{\rm heat}$) is defined as the ratio between the increment of internal energy of the fuel core ($\Delta E_{\rm core}$) by REB-induced heating and the energy of the heating laser ($E_{\rm L}$).

Integrated experiments [5–8] and simulations [9–12] to evaluate directly the overall heating efficiency as well as basic experiments [13] have been performed to understand generation [14–17] and transport [18,19] of REBs. Novel ideas have been proposed to increase the coupling efficiency, for example, guiding of the REB by externally imposed [9,20–22] and/or spontaneously generated magnetic fields by double laser pulses [23,24] or by resistivity gradients induced by plasma temperature gradients [25] or material boundaries [26,27]. However, most of the basic experiments were carried out with solid targets in planar geometry. In a more realistic FI scenario, the REB transports through a plasma whose properties are, in general, very different from those of a cold

solid matter; even in a basic FI experiment, plasma conditions mimicking the integrated experiments are required to obtain meaningful results for the FI-integrated experiment.

Our strategy to achieve the FIREX goal is as follows. First step is a basic experiment, in which energy conversion ratio from the heating laser to the REB, energy distribution, and divergence of the REB are measured to estimate the heating efficiency and are optimized to increase the efficiency. Second step is a heating experiment, in which optimized REB heats a dense plasma to measure directly the heating efficiency and to clarify physics hidden in the basic experiment. In the heating experiment, the dense plasma is generated with a solid ball compressed by converging spherical shock wave, because this scheme is more suitable than a thin shell implosion owing to its hydrodynamical stability, creditability, and reproducibility with the current GEKKO laser system. Final step is an integrated experiment, in which more dense plasma generated by the thin shell implosion is heated with the REB for the demonstration of the fast ignition scheme. This paper focuses on the basic experiment as a step to the heating experiment.

II. SIMPLE MODEL TO EVALUATE HEATING EFFICIENCY WITH MEASURED VALUES IN BASIC EXPERIMENT

Experimental platforms have been developed to study generation and transport of REB for FI. A novel target constituted by a gold cone-attached plastic hemishell is mounted on a high-Z metal block, 1.2 mm $\times$ 1.0 mm $\times$ 1.0 mm in size [see Fig. 1(a)], was designed for the basic experiment. The metal block consists of two layers: 0.2-mm-thick Sn and
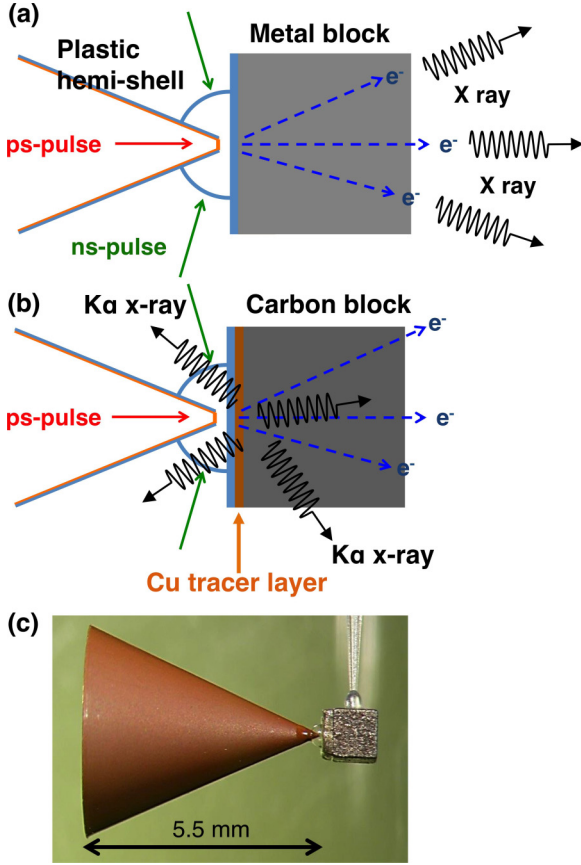
*sfujioka@ile.osaka-u.ac.jp

FIG. 1. (Color online) Schematic drawings [(a) and (b)] and a photograph (c) of a target used in experiments. (a) A gold cone attached hemishell is mounted on a high-Z (Sn and Ta) metal block. REB generated at the cone-tip is converted into $K\alpha$ and Bremsstrahlung x-rays in the block. Absolute spectrum and angular distribution of x-rays were measured to determine the absolute number and energy distribution of the REB. (b) A Cu tracer layer is located on a C block to measure spatial profile of the REB by measuring Cu-$K\alpha$ x-ray emission profile. The C block is a REB damper to prevent Cu-$K\alpha$ emission by refluxing electrons around the tracer layer.

1.0-mm-thick Ta. Nanosecond laser beams irradiate the hemishell to produce a rarefied plasma surrounding the cone, which density and temperature profiles are similar to those characteristic of a FI-integrated experiment except for existence of a dense fuel core. The REB transports through the cone tip and the rarefied plasma and it propagates through the metal block instead of a fuel core, where part of its energy is converted to bremsstrahlung and $K\alpha$ x-ray photons. The REB parameters, namely E_{REB}, T_{REB}, and r_{REB}, are measured in the block region, this means these parameters defined as the values not at the generation region but after transport through the cone tip and the rarefied plasma, here E_{REB}, T_{REB}, and r_{REB} are total kinetic energy carried by the REB, a slope temperature of the REB energy distribution, and REB radius, respectively. The values of E_{REB} and T_{REB} were obtained from a comparison between the absolute x-ray spectra emitted from the metal block and Monte Carlo calculation (Geant4 [28] and/or PHITS codes [29]) of particle-matter interaction. The value of r_{REB}

was measured by measuring the size of the $K\alpha$ emission from a Cu tracer layer on a C block ($1 \times 1 \times 1$ mm^3) instead of a metal block [see Fig. 1(b)].

Although the heating efficiency depends on a complex variety of collective and collisional phenomena, as well as on the specific REB parameters, we can sum the physics up to several measurable parameters for simplicity. This simplified relation between the heating efficiency and the measurable plasma and beam parameters is represented as follow:

$$\eta_{\text{heat}} = \frac{\Delta E_{\text{core}}}{E_{\text{L}}} = \eta_{\text{REB}}\eta_{\text{col}}\eta_{\text{dep}} = \frac{E_{\text{REB}}}{E_{\text{L}}} \frac{\pi r_{\text{core}}^2}{\pi r_{\text{REB}}^2} \frac{2\rho_{\text{core}}r_{\text{core}}}{R_{\text{REB}}}$$

$$= \frac{E_{\text{REB}}}{E_{\text{L}}} \frac{\pi r_{\text{core}}^2}{\pi r_{\text{REB}}^2} \frac{2\rho_{\text{core}}r_{\text{core}}}{0.6T_{\text{REB}}}, \tag{1}$$

here η_{REB}, η_{col}, and η_{dep} are, respectively, the energy conversion ratio from laser to REB, the probability of collision between the REB and the fuel core, and the fraction of energy deposited in the fuel core from the REB. More specifically η_{REB} is the ratio between total kinetic energy carried by the REB after the transport (E_{REB}) and E_{L}, η_{col} is approximated based on geometrical consideration as the ratio between the geometrical cross-section of the fusion fuel core (πr_{core}^2) and that of the REB (πr_{REB}^2) at the core position, and η_{dep} is approximated as the ratio between the areal density of the fusion fuel core ($2\rho_{\text{core}}r_{\text{core}}$) and the average range of the REB in the compressed core (R_{REB}). An approximated relation of Eq. (11) in Ref. [30], R_{REB} [g/cm^2] $= 0.6 f_{\text{R}} T_{\text{REB}}$ [MeV], is used to calculate the R_{REB} from the experimentally measurable parameter (T_{REB}), here f_{R} is an adjustable parameter, set to 1 in the standard model.

III. CHARACTERIZATION OF RELATIVISTIC ELECTRON BEAM GENERATED WITH MIMICKING FAST-IGNITION CONDITIONS

A. Target and laser conditions

Figure 1 shows schematics [(a) and (b)] and a photograph (c) of targets used in the basic experiment. A 7-μm-thick and 250-μm-radius hemishell made of deuterized plastic (CD) was imploded by three laser beams of GEKKO-XII laser facility. Surface of the block was coated with a 2-μm-thick parylene (CH) layer to prevent high-Z contamination from a block material to an imploded plasma. Energy, wavelength, pulse shape, and pulse duration of the laser beams were 250 $\pm$ 10 J/beam, 0.53 μm, Gaussian, and 1.3 ns of full-width half-maximum (FWHM), respectively. The inner cone tip was irradiated by the LFEX laser pulses, whose energy, wavelength, duration, and intensity were $E_{\text{L}} = 820 \pm 150$ J, $\lambda_{\text{L}} = 1.053$ μm, $t_{\text{L}} = 1.4 \pm 0.1$ ps (FWHM), and $I_{\text{L}} = (3.0 \pm 0.6) \times 10^{19}$ W/cm^2, respectively.

Outer surface of the 7-μm-thick gold cone was covered with a 2-μm-thick CH layer to prevent gold plasma generation because x-rays from a gold plasma may preheat a hemishell. In the GEKKO system, $F/3$ laser focusing lens locate just behind frequency doubling potassium dihydrogen phosphate (KDP) crystals, 1.053-μm light unconverted in a KDP crystal also passes through the lens and is focused loosely on a target. Diameter of a loosely focused unconverted 1.053-μm light is about 8 mm at the target position. Its intensity is about
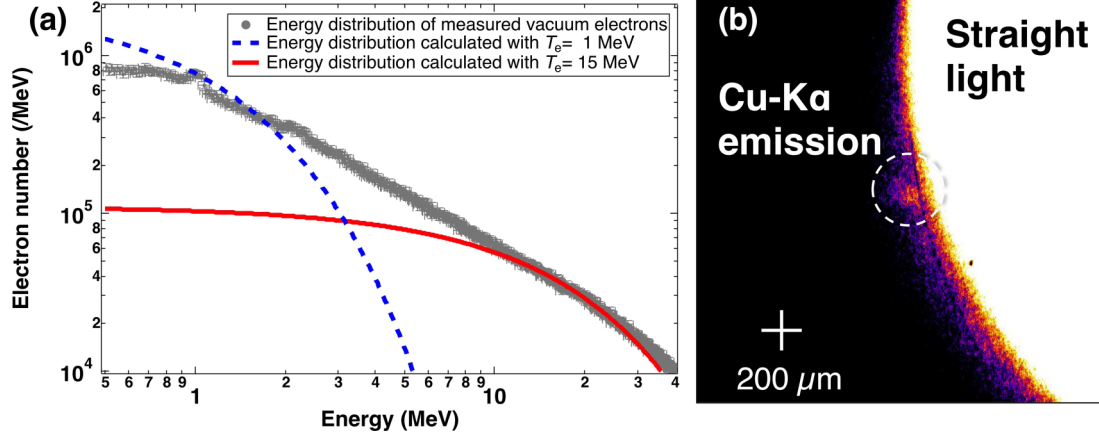
FIG. 2. (Color online) (a) Comparison between energy distribution of vacuum electrons and that obtained from hard x-ray spectrum. Gray dots represent energy distributions of energetic electrons, so-called vacuum electrons, escaped from the metal block into vacuum, which were measured with an electron energy spectrometer. Error of vacuum electron numbers is $\pm 5\%$ owing to uncertain of analyzer detector response for electrons, and error of electron energy is $\pm 4.5\%$ owing to uncertain of its calibration. Blue broken and red solid lines are Boltzmann distributions calculated with $T_{REB1} = 1$ and $T_{REB2} = 15$ MeV of slope temperature and $A = 0.95$ of relative coefficient. Slope temperature of higher-energy component (T_{REB2}) was obtained by fitting the energy distribution of the vacuum electrons in the range of $E > 10$ MeV with the function $[\exp(-E/T_{REB2})]$. The lower-energy component (T_{REB1}) and coefficient (A) were evaluated from measured hard x-ray signal. (b) Cu-Kα emission from a Cu tracer layer was measured with a spherically bent quartz crystal. The spot diameter corresponds to REB diameter at the dense fuel core position. The radius of the $K\alpha$ spot highlighted by the circle shows $r_{REB} = 40 \pm 10\,\mu$m FWHM. The white cross is a spatial scale of 200 μm in the image plane.

5×10^{11} W/cm^2, which is high enough to produce a long-scale plasma. Length of the cone was determined to be 5.5 mm for protecting a inner cone wall from direct illumination of the unconverted 1.053 μm light.

The plasma density profile around the cone tip was measured with a time-resolved x-ray backlight imaging. Mass density of the CD plasma concentrated at the cone tip was $8^{+4}_{-2} \times 10^{-2}$ g/cm^3 at the LFEX injection time. The REB emitted from the cone tip travels in a hot and rarefied CD plasma between the tip and the block. Two stream instability effect [31] is small compared to the Weibel instability in the basic experiment owing to the return current velocity being roughly $0.2c$ (c is speed of light) because $2.6^{+1.3}_{-0.6} \times 10^{22}$ cm^{-3} of electron density (fully ionized case with ionization degree 3.5) is 5 times higher than the relativistic critical density $n_{cr} = (1 + a_0^2)^{1/2}n_c = (5.0 \pm 0.47) \times 10^{21}$ cm^{-3} for the heating laser intensity ($a_0 = 4.9 \pm 0.48$), here a_0 and n_c are the dimensionless amplitude of the laser field in vacuum and the classical critical density.

B. Energy distribution of relativistic electron beam

Bremsstrahlung x rays were measured using high energy x-ray spectrometers (HEXSs) [32], the spectrometers consist of K-edge and differential x-ray filters and use imaging plates (IPs) as detectors. Three HEXSs were set at 180°, 159.1°, and 110.9° from the LFEX laser axis. The dependence of the doses on the IP order in the stack was compared with Monte Carlo calculations, in which a Boltzmann distribution $[f(E)]$ with two slope temperatures (T_{REB1}, T_{REB2} and $T_{REB1} < T_{REB2}$), namely $f(E) = A\exp(-E/T_{REB1}) + (1 - A)\exp(-E/T_{REB2})$, and a single divergence angle (θ_{div}) of the

REB were assumed. Here A and E are the relative coefficient and the electron kinetic energy, respectively.

Energy distribution of the vacuum electrons, which escape from the metal block into vacuum, was measured with an electron energy analyzer. Slope temperature of higher energy component (T_{REB2}) was obtained by fitting the energy distribution of the vacuum electrons (gray dots in Fig. 2) in the range of $E > 10$ MeV with the function $[\exp(-E/T_{REB2})]$ for reducing indefiniteness of the fitting process. The lower energy component (T_{REB1}) cannot be obtained from the vacuum electron distribution, because the sheath field generated at the metal block surfaces affects strongly motion of the low-energy REB. Hard x-ray spectrum was used to obtain T_{REB1} inside the metal block. Error of vacuum electron numbers is $\pm 5\%$ owing to uncertainty of analyzer detector response (IP) for electrons, and error of electron energy is $\pm 4.5\%$ owing to uncertainty of its calibration.

Fit residual value between the experimentally measured bremsstrahlung x-ray signal and Monte Carlo calculations is defined as $\frac{1}{3}\sum_{N=1}^{3}\sqrt{\sum_{M=1}^{12}((D_{M,N}^{expt} - D_{M,N}^{cal})/D_{M,N}^{expt})^2}$; here N, M, $D_{M,N}^{expt}$, and $D_{M,N}^{cal}$ are label number of the HEXS ($N = 1, 2, 3$), IP layer number ($M = 1, 2,..., 12$), experimentally obtained and calculated doses of Mth IP in Nth HEXS. The minimum residual value was obtained with $A = 0.95$, $T_{REB1} = 1.0$ MeV, and $T_{REB2} = 15$ MeV and divergence angle of $\theta_{div} = 41°$ FWHM. This divergence angle was evaluated from the spatial profile of $K\alpha$ fluorescence induced by the REB as discussed later.

Figures 3(a)–3(c) show comparisons between calculations and x-ray doses recorded in IP layers of HEXS located at (a) 180°, (b) 159.1°, and (c) 110.9° from the LFEX laser axis. The curves shown in Figs. 3(a)–3(c) are computed for the following
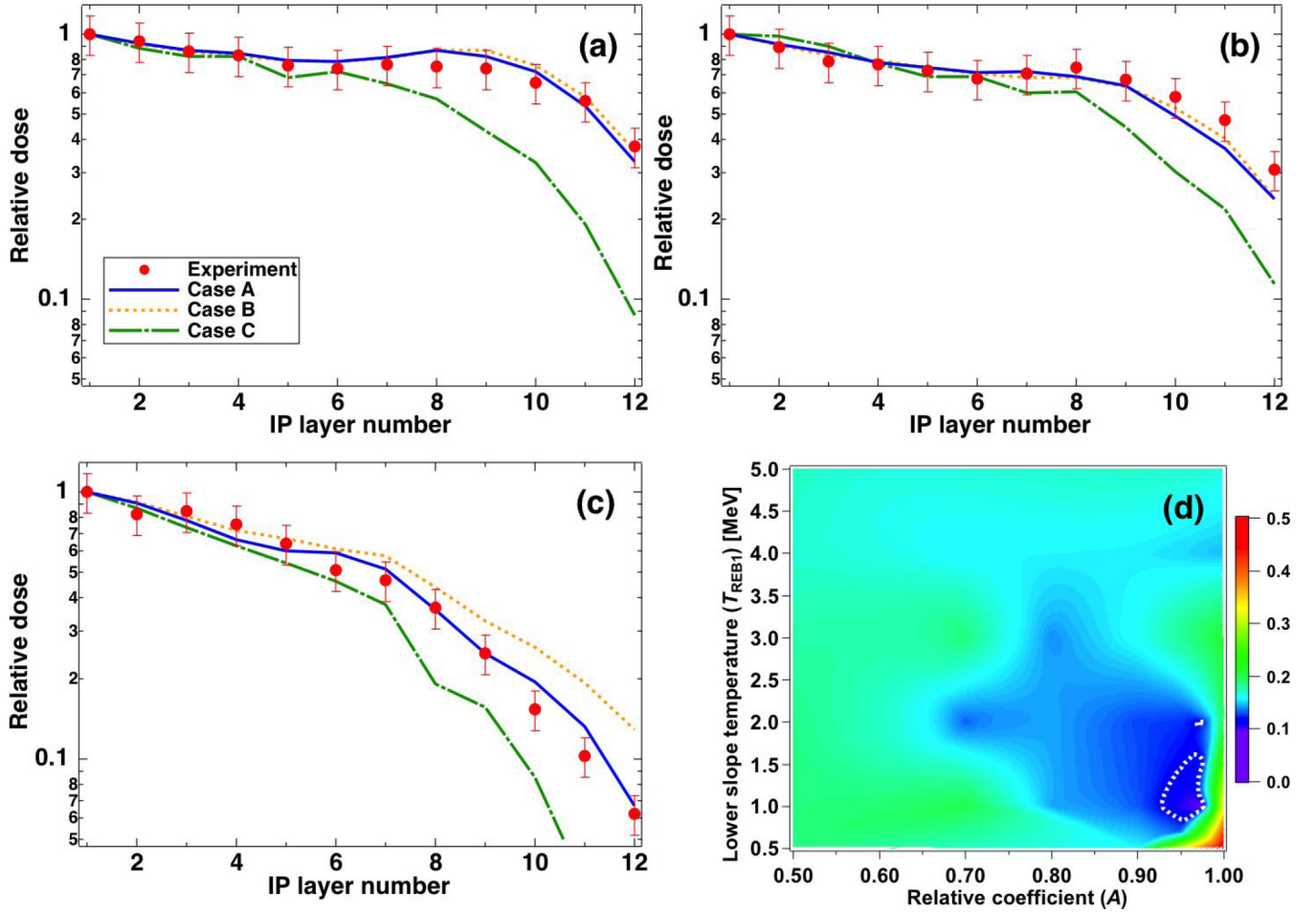
FIG. 3. (Color online) Relative x-ray doses (red solid circles) recorded on imaging plates in HEXSs located at (a) 180°, (b) 159.1°, and (c) 110.9° from the LFEX laser incident axis were compared with Monte Carlo calculations. The curves were calculated for three cases of REB energy distribution; [Case A (blue solid line)] $A = 0.95$, $T_{REB1} = 1$ MeV, and $T_{REB2} = 15$ MeV; [Case B (orange broken line)] $A = 0.5$, $T_{REB1} = 1$ MeV, and $T_{REB2} = 15$ MeV; [Case C (green dash-dot line)] $A = 1$, $T_{REB1} = 1$ MeV, respectively. Errors in the measured doses are caused by uncertain of IP calibration for x rays. (d) Sensitivity of fitting of calculations to the experimental doses for varying relative coefficient (A) and lower slope temperature (T_{REB1}) with fixed higher slope temperature ($T_{REB2} = 15$ MeV) and divergence angle ($\theta_{div} = 41°$ FWHM). The fitting residual values defined as in the text are color coded and the white broken line is a contour line of 0.12.

three cases; [Case A (blue solid line)] $A = 0.95$, $T_{REB1} = 1$ MeV, $T_{REB2} = 15$ MeV, and $\theta_{div} = 41°$; [Case B (orange broken line)] $A = 0.5$, $T_{REB1} = 1$ MeV, $T_{REB2} = 15$ MeV, and $\theta_{div} = 41°$; [Case C (green dash-dot line)] $A = 1$, $T_{REB1} = 1$ MeV, and $\theta_{div} = 41°$, respectively. Figure 3(d) shows the fit residual values calculated for given relative coefficients (A) and lower component (T_{REB1}) of REB energy distributions with fixing $T_{REB2} = 15$ MeV and $\theta_{div} = 41°$. The white broken line in Fig. 3(d) is the contour of 0.12. Errors in the measured doses are caused by uncertainty of IP response calibration for hard x rays. Blue broken and red solid lines in Fig. 2 are Boltzmann distributions calculated with $T_{REB1} = 1$ and $T_{REB2} = 15$ MeV of slope temperature and $A = 0.95$ of relative coefficient.

Energy conversion efficiency from laser to REB after the transport was estimated to be $\eta_{REB} = E_{REB}/E_L = 0.38 \pm 0.06$ from the measured absolute number of the bremsstrahlung x-ray photons. $K\alpha$ x rays from Sn ($h\nu = 25$ keV) and Ta ($h\nu = 58$ keV) layers were also measured with a Laue-type crystal spectrometer [33]. Only Sn-$K\alpha$ signal was measurable

while the Ta-$K\alpha$ signal was buried in the background noise; this result is consistent with the electron energy distribution obtained from the HEXS measurement. η_{REB} was obtained from the absolute intensity of the Sn-$K\alpha$ to be 0.40 ± 0.07.

C. Spatial profile of relativistic electron beam

For measurement of the REB radium (r_{REB}), we used a 10-μm-thick Cu tracer layer on the front surface of a C block ($1 \times 1 \times 1$ mm^3) instead of a metal block as shown in Fig. 1. The REB radius was measured as a spot size of the $K\alpha$ emission from the Cu tracer layer. Distance between the Cu tracer layer and the cone tip is 60 ± 10 μm. This distance is the same as between the cone tip and the center of the fuel capsule in the FI-integrated experiment. Therefore, the spatial extension of the Cu-$K\alpha$ image corresponds to that of the REB at the fuel core. The C block was attached as a REB dumper to prevent Cu-$K\alpha$ emission induced by refluxing electrons around the tracer layer. Figure 4 shows a comparison between
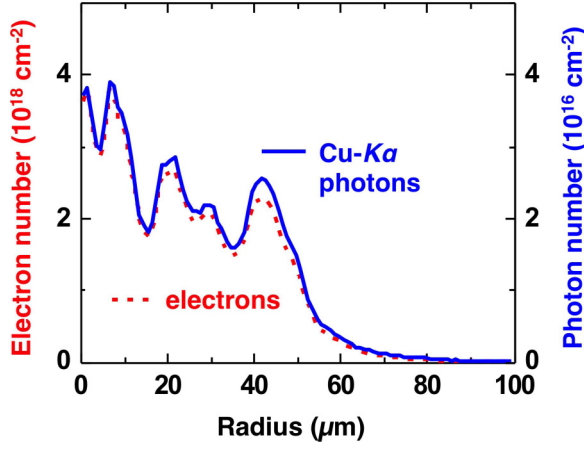
FIG. 4. (Color online) Comparison between computed spatial distributions of REB (red broken line) and $K\alpha$ emission profile (blue solid line). The REB profile is almost identical to $K\alpha$ emission profile calculated with consideration of cross-section and spatial and energy distributions of the REB after transport through the cone tip and the plasma. Details of the REB transport simulation is described in the text.

computed spatial distributions of REB (red broken line) at the tracer layer position and Cu-$K\alpha$ emission (blue solid line); details of the REB transport simulation is described later. The Cu-$K\alpha$ emission pattern was calculated with cross-section [34] and energy and spatial distributions of the REB. We conclude that spot size of the $K\alpha$ emission can be used as the REB size at the tracer layer position, which corresponds to a fuel core position, after the transport through the cone tip and the rarefied plasma.

Spherically bent quartz crystal was used to image Cu-$K\alpha$ x rays ($h\nu = 8.0$ keV) on an IP. Figure 2(b) shows the image obtained with the tracer target and imager. Strong emission labeled with straight light is cased by x rays that come directly from a plasma without being reflected by the quartz crystal. The radius of the $K\alpha$ spot highlighted by the circle is $r_{REB} = 40 \pm 10$ μm FWHM. This leads to $\theta_{div} = 41° \pm 17°$ with the assumption that source diameter and transport region length are equal to the diameter of cone tip (35 μm) and the distance between the cone tip and the tracer layer.

It was confirmed that REB transport is not modulated by structures of the tracer target by using a simulation code [35], in which the transport is solved by particle scheme instead of Fokker-Planck equation. REB parameters used in this simulation were determined based on the experiment. Energy and duration of the REB are $E_{REB} = 320$ J and $t_{REB} = 1.5$ ps, respectively. Angular distribution, energy distribution, and spatial profile of the REB are, respectively, $f(\theta) \propto \exp(-\log(2)(\theta/40°)^4)$, $f(E) \propto 0.95\exp[-(E/1[\text{MeV}])] + 0.05\exp[-(E/15[\text{MeV}])]$ and $f(r) \propto \exp[-\log(2)(r/17.5[\mu\text{m}])^4]$ at the injection position [$z = 0$ of Fig. 5(a)]; here θ, E, and r are direction angle, energy, and radius of electrons in the beam.

Figure 5(a) shows two-dimensional (2D) profile of mass density in a tracer target at the LFEX injection timing, which was calculated with a 2D radiation-hydrodynamic simulation code PINOCO-2D [36]. Figures 5(b) and 5(c) show REB
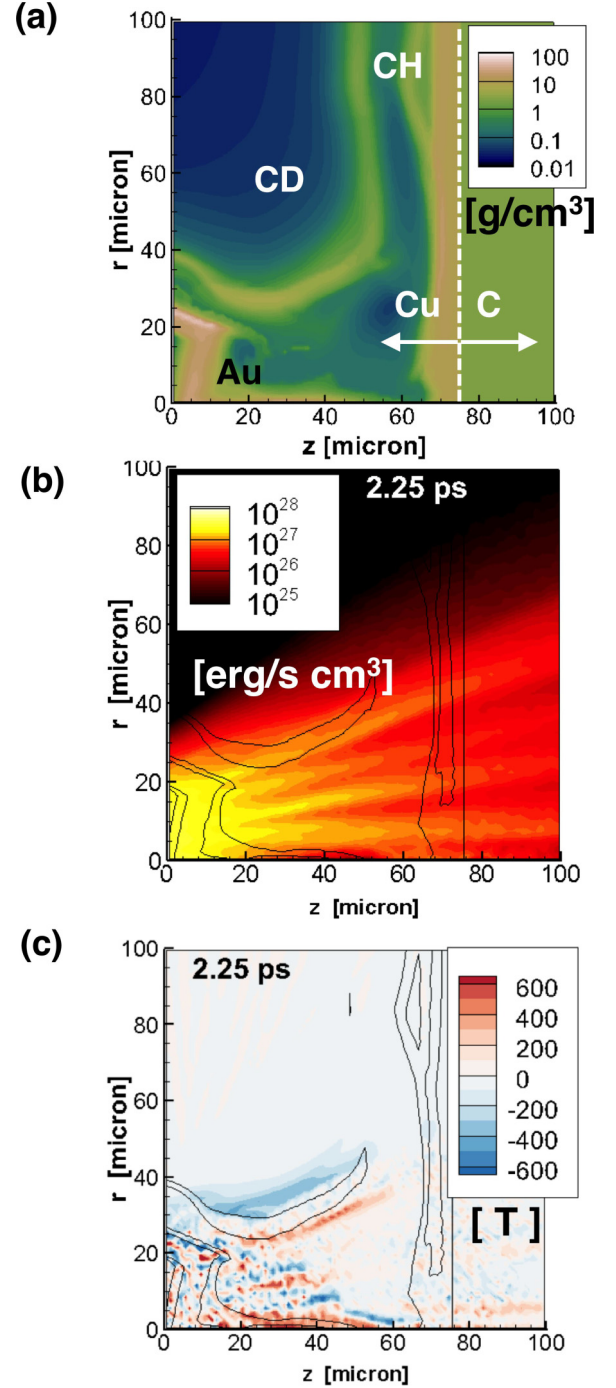

FIG. 5. (Color online) REB transport was computed in a tracer target with a simulation code to confirm that is not modulated by structures of the tracer target. (a) Two-dimensional (2D) density profile of the REB transport region that was calculated with a 2D radiation-hydrodynamic simulation code. Computed 2D profiles of REB energy density in erg/s cm^3 unit (b) and strength of azimuthal magnetic field in T unit (c) generated by the REB itself. Structures of the tracer target do not modulate the REB transport.

energy density (erg s^{-1} cm^{-3}) and strength of azimuthal magnetic field (T) generated spontaneously by the REB itself at the peak beam intensity timing. Although beam filaments due to resistive instability is observed, the REB travels in

the rarefied plasma to the tracer layer with keeping its initial divergence angle. It is clear that REB transport is not affected by the material boundaries between the CH and CD plasmas, the CH plasma and the Cu tracer layer, and the Cu tracer layer and the C damper.

Note that divergence angle may be overestimated in this estimation. Because energy majority of the REB were generated in a long-scale plasma as discussed in Sec. V, it is highly possible that initial diameter of the REB is larger than the cone-tip diameter and transport region is longer than the distance between the cone tip and the tracer layer. However, initial divergence angle of the REB affects weakly on angular distribution of hard x-ray signal measured with three HEXSs because REB are scattered multiply by bulk electrons in the Sn and Ta metal block.

IV. EVALUATION OF HEATING EFFICIENCY FOR HEATING EXPERIMENT

A. Dense plasma production with spherically converging shock wave

To generate dense plasma in the heating experiment, nine GEKKO-XII beams where focused on a solid CD sphere. The ablation pressure generated by the pulses drives a converging spherical shock. According to the Guderley's self-similar solution, the spherically converging strong shock wave can compress an ideal gas plasma (specific heat capacity ratio $\gamma = 5/3$) up to 34 times of the initial density. Although the compressibility is significantly lower than that expected in thin-shell implosion, the converging shock compression of a solid ball is more hydrodynamically stable than the thin-shell implosion.

The spherical CD ball, whose initial diameter was $190 \pm 10\,\mu$m, was imploded by nine beams of GEKKO-XII. The three remaining GEKKO-XII beams were focused on a Ti foil to produce Ti-Heα x rays ($h\nu = 4.85$ keV) for backlighting. The laser pulse is temporally Gaussian-shaped having 1.1 ns FWHM duration, 0.53 μm of wavelength, and 240 J of energy per beam. Figure 6 shows x-ray radiograph of the compressed
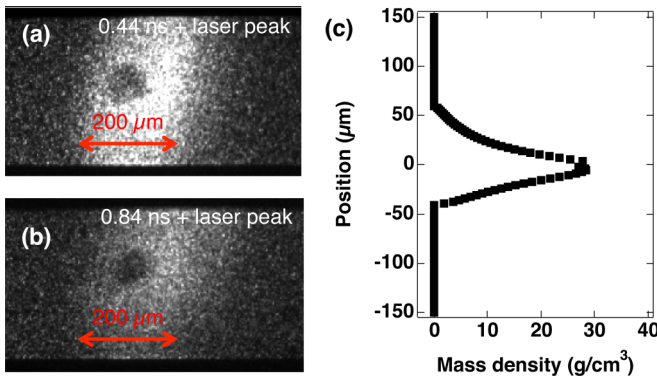

FIG. 6. (Color online) X-ray backlight images of solid CD ball compressed by nine laser beams at 0.44 and 0.84 ns after the peak of the laser pulse. Nine beams of GEKKO-XII laser irradiate asymmetrically on the CD ball. (c) Density profile was obtained from the shadow image after Abel inversion. Peak density and areal density are 22 ± 6 g/cm^3 and 54 ± 9 mg/cm^2, respectively.

CD ball backlit by Ti-Heα x rays. Density and areal density were measured with x-ray backlighting technique to be $\rho_{\text{core}} = 22 \pm 6$ g/cm^3, $\rho_{\text{core}} r_{\text{core}} = 54 \pm 9$ mg/cm^2, then $r_{\text{core}} = 25 \pm 8\,\mu$m around the maximum compression timing.

B. Evaluation of heating efficiency with experimentally measured values

Heating efficiency was estimated for the heating experiment with the following values were obtained from the series of the basic experiments: $\eta_{\text{REB}} = E_{\text{REB}}/E_L = 0.39 \pm 0.07$, $r_{\text{core}} = 25 \pm 8\,\mu$m, $r_{\text{REB}} = 40 \pm 10\,\mu$m, $\rho_{\text{core}} = 22 \pm 6$ g/cm^3, $A = 0.95$, $T_{\text{REB1}} = 1$ MeV, and $T_{\text{REB2}} = 15$ MeV, then $\eta_{\text{col}} = 0.38 \pm 0.22$ and $\eta_{\text{dep}} = 0.025 \pm 0.004$. The coupling efficiency was only $0.37 \pm 0.23\%$. Note that the two temperatures assumption modify the fraction (η_{dep}) of energy deposited in the fuel core from the REB of Eq. (1) as

$$\eta_{\text{dep}} = \frac{AT_{\text{REB1}}^2}{AT_{\text{REB1}}^2 + (1-A)T_{\text{REB2}}^2} \frac{2\rho_{\text{core}}r_{\text{core}}}{0.6T_{\text{REB1}}}$$
$$+ \frac{(1-A)T_{\text{REB2}}^2}{AT_{\text{REB1}}^2 + (1-A)T_{\text{REB2}}^2} \frac{2\rho_{\text{core}}r_{\text{core}}}{0.6T_{\text{REB2}}}; \quad (2)$$

here the first and second terms represent the fractions of energy deposition in the core from the T_{REB1} and T_{REB2} components of the REB, respectively, because of $\int_0^\infty E e^{-\frac{E}{T}} dE = T^2$.

V. DISCUSSION FOR INCREASING HEATING EFFICIENCY

More accurate evaluation of heating efficiency was performed with a simulation code [35] of the REB transport in a plasma. REB parameters used in this simulation are the same as parameters of REB transport calculation in a tracer target. Density profile, areal density, and electron and ion temperatures of the core plasma are, respectively, $\rho(r) = 22[\text{g/cm}^3] \exp[-\log(2)(r/25[\mu\text{m}])^6]$, 54 mg/cm^2, and $T_i = T_e = 300$ eV, those are determined according to the x-ray backlight measurement and a hydrodynamics simulation.

Figures 7(a) and 7(b) show a schematic of simulation conditions and temperature profile at 4 ps after the REB injection time with the above parameters. This calculation shows that $\eta_{\text{col}}\eta_{\text{dep}}$ is 1.3%, while the simple model gives 1.0%. The differences are caused mainly by collective effects, i.e., spontaneous generation of magnetic field and ohmic heating by return current, those are initiated by the forward REB current, which is not considered in the simple model.

Comparison of the measured slope temperature (T_{REB1} and T_{REB2}) of the REB with the reported scaling is discussed here. Scaling reported by Wilks [37], Beg [38], Tanimoto [39], and Haines [40] give 1.3 ± 0.2, 0.7 ± 0.04, 1.3 ± 0.1, and 0.7 ± 0.05 MeV of the temperature generated by LFEX laser intensity [$I_L = (3.0 \pm 0.6) \times 10^{19}$ W/cm^2]. Slope temperature of lower-energy component ($T_{\text{REB1}} = 1$ MeV) is not so far from the scaling values; however, the higher component one ($T_{\text{REB2}} = 15$ MeV) is one order of magnitude larger than the scaling value. And also the higher component carries 92% of the total kinetic energy of the REB as $(1 - A)T_{\text{REB2}}^2/[AT_{\text{REB1}}^2 + (1-A)T_{\text{REB2}}^2] = 0.92$. These energetic electrons may be generated by laser-plasma interaction in a
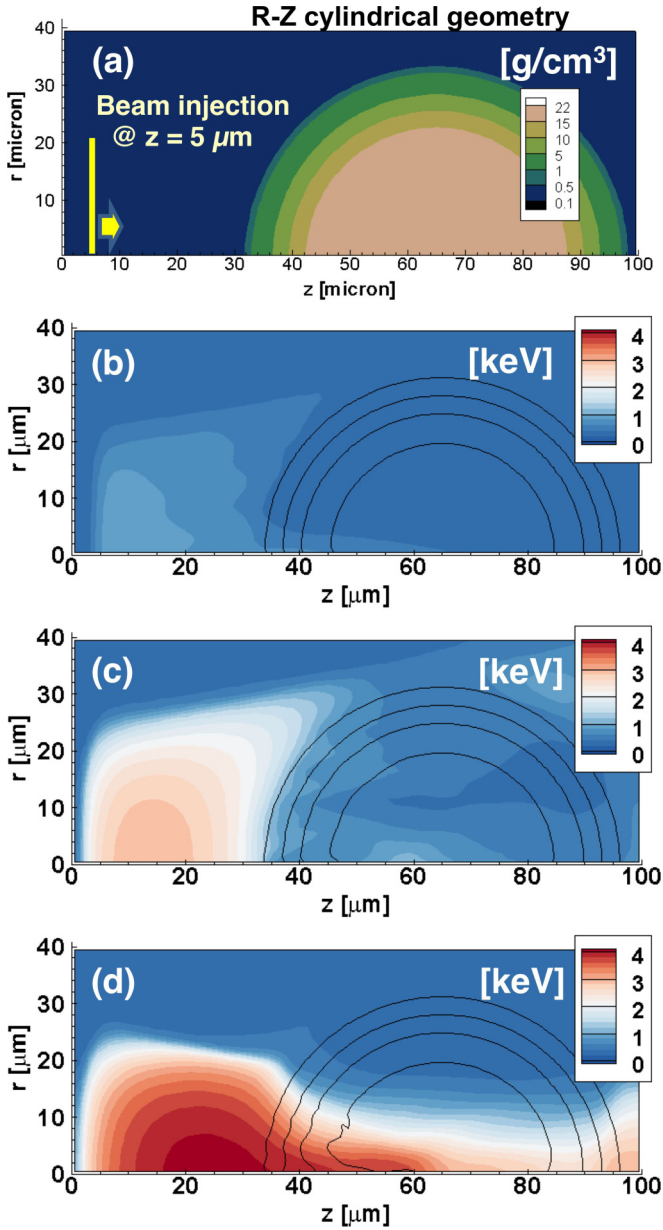
The simulation indicates that the efficiency increases up to $\eta_{col}\eta_{dep} = 11\%$ by suppressing higher-temperature component, while the simple model shows 6.8%. Furthermore, the radius of the REB is larger than the one of the fuel core; this is caused by the divergence of the REB, resulting in a reduction of η_{col}. If the divergence of the REB is $0°$, the efficiency increases up to $\eta_{col}\eta_{dep} = 27\%$ with further help of spontaneous-generation of magnetic field as shown in Fig. 7(d), while the simple model shows 18%.

VI. SUMMARY

The basic experiment was carried out to evaluate the heating efficiency of the FI scheme. The experimental results clarify that there are difficulties in the fast ignition scheme, as the "unstoppable" REB generated by laser-plasma interactions. The REB is too energetic to heat the fuel core under the present experimental conditions, which decreases the value of η_{dep}. Although complexity of REB generation and transport are ignored in this model, the experimental platform gives a reasonable guideline for future experiment design. We are now introducing a plasma mirror [44,45] in the LFEX laser system to exclude the pedestal on the target surface and to suppress the generation of high-energy component of REB with keeping high η_{REB}. Additionally, divergence of the REB results is a potential difficulty in our experiment; one candidate scheme to suppress its divergence is to apply more than 1 kT of external magnetic field [9] in the transport region to guide the REB to the fuel core. Generation of a 1-kT magnetic field has already been demonstrated by using capacitor-coil targets on GEKKO-XII laser facility [22]. Enhancement of the heating efficiency by the magnetic field will also be tested in the basic experimental platform. According to the transport calculation and the simple model, 10% of η_{heat} is achievable by the current GEKKO and LFEX laser system with the success of the above improvements.

FIG. 7. (Color online) Transport of the REB in a fuel core was computed with a simulation code. (a) Density profile of the fuel core used in the computation. Temperature profile of bulk electrons heated by experimentally characterized REB (b), REB with 1 MeV single slope temperature and $40°$ divergence angle (c), and REB with 1 MeV single slope temperature and $0°$ divergence angle (d). Units of the color (gray) scales are g/cm^3 (a) and keV (b, c, d). The energy coupling efficiency from the REB to the core ($\rho > 1$ g/cm^3) are 1.3% (b), 11% (c), and 27% (d), respectively.

long-scale preformed plasma and/or interaction between the oblique incident laser and a solid on the inner cone wall. The vacuum electron energy spectrum is close to a power-law shape, as shown in Fig. 2; this may indicate high-energy electrons were accelerated stochastically [41–43] by laser field in a long-scale plasma. The long-scale plasma is generated by the pedestal of the heating laser pulse. Typical peak intensity and duration of the pedestal of the LFEX were 10^{15} W/cm^2 and 200 ps FWHM during this experimental series.

[1] N. G. Basov, S. Y. Gus'kov, and L. P. Feokistov, J. Sov. Laser Res. **13**, 396 (1992).

[2] M. Tabak, J. Hammer, M. E. Glinsky, W. L. Kruer, S. C. Wilks, J. Woodworth, E. M. Campbell, M. D. Perry, and R. J. Mason, Phys. Plasmas **1**, 1626 (1994).

[3] H. Azechi, K. Mima, Y. Fujimoto, S. Fujioka, H. Homma, M. Isobe, A. Iwamoto, T. Jitsuno, T. Johzaki, R. Kodama *et al.*, Nucl. Fusion **49**, 104024 (2009).

[4] N. Miyanaga, H. Azechi, K. A. Tanaka, T. Kanabe, T. Jitsuno, J. Kawanaka, Y. Fujimoto, R. Kodama, H. Shiraga, K. Knodo *et al.*, J. Phys. IV France **133**, 81 (2006).

[5] R. Kodama, P. A. Norreys, K. Mima, A. E. Dangor, R. G. Evans, H. Fujita, Y. Kitagawa, K. Krushelnick, T. Miyakoshi, N. Miyanaga *et al.*, Nature **412**, 798 (2001).

[6] W. Theobald, A. A. Solodov, C. Stoeckl, K. S. Anderson, R. Betti, T. R. Boehly, R. S. Craxton, J. A. Delettrez, C. Dorrer, J. A. Frenje *et al.*, Phys. Plasmas **18**, 056305 (2011).

[7] H. Shiraga, S. Fujioka, M. Nakai, T. Watari, H. Nakamura, Y. Arikawa, H. Hosoda, T. Nagai, M. Koga, H. Kikuchi *et al.*, Plasma Phys. Controlled Fusion **53**, 124029 (2011).

[8] H. Shiraga, H. Nagatomo, W. Theobald, A. A. Solodov, and M. Tabak, Nucl. Fusion **54**, 054005 (2014).

[9] D. J. Strozzi, M. Tabak, D. J. Larson, L. Divol, A. J. Kemp, C. Bellei, M. M. Marinak, and M. H. Key, Phys. Plasmas **19**, 072711 (2012).

[10] T. Johzaki, H. Nagatomo, A. Sunahara, H.-B. Cai, H. Sakagami, Y. Nakao, and K. Mima, Nucl. Fusion **51**, 073022 (2011).

[11] A. Kemp, F. Fiuza, A. Debayle, T. Johzaki, W. Mori, P. Patel, Y. Sentoku, and L. Silva, Nucl. Fusion **54**, 054002 (2014).

[12] A. Robinson, D. Strozzi, J. Davies, L. Gremillet, J. Honrubia, T. Johzaki, R. Kingham, M. Sherlock, and A. Solodov, Nucl. Fusion **54**, 054003 (2014).

[13] P. Norreys, D. Batani, S. Baton, F. N. Beg, R. Kodama, P. Nilson, P. Patel, F. Pérez, J. Santos, R. Scott *et al.*, Nucl. Fusion **54**, 054004 (2014).

[14] J. Green, V. Ovchinnikov, R. Evans, K. Akli, H. Azechi, F. Beg, C. Bellei, R. Freeman, H. Habara, R. Heathcote *et al.*, Phys. Rev. Lett. **100**, 015003 (2008).

[15] T. Ma, H. Sawada, P. K. Patel, C. D. Chen, L. Divol, D. P. Higginson, A. J. Kemp, M. H. Key, D. J. Larson, S. Le Pape *et al.*, Phys. Rev. Lett. **108**, 115004 (2012).

[16] C. D. Chen, A. J. Kemp, F. Pérez, A. Link, F. N. Beg, S. Chawla, M. H. Key, H. McLean, A. Morace, Y. Ping *et al.*, Phys. Plasmas **20**, 052703 (2013).

[17] F. Pérez, A. J. Kemp, L. Divol, C. D. Chen, and P. K. Patel, Phys. Rev. Lett. **111**, 245001 (2013).

[18] B. Vauzour, J. J. Santos, A. Debayle, S. Hulin, H.-P. Schlenvoigt, X. Vaisseau, D. Batani, S. D. Baton, J. J. Honrubia, P. Nicolaï *et al.*, Phys. Rev. Lett. **109**, 255002 (2012).

[19] S. Chawla, M. S. Wei, R. Mishra, K. U. Akli, C. D. Chen, H. S. McLean, A. Morace, P. K. Patel, H. Sawada, Y. Sentoku *et al.*, Phys. Rev. Lett. **110**, 025001 (2013).

[20] H.-B. Cai, S.-P. Zhu, and X. T. He, Phys. Plasmas **20**, 072701 (2013).

[21] S. Fujioka, Z. Zhang, N. Yamamoto, S. Ohira, Y. Fujii, K. Ishihara, T. Johzaki, A. Sunahara, Y. Arikawa, K. Shigemori *et al.*, Plasma Phys. Controlled Fusion **54**, 124042 (2012).

[22] S. Fujioka, Z. Zhang, K. Ishihara, K. Shigemori, Y. Hironaka, T. Johzaki, A. Sunahara, N. Yamamoto, H. Nakashima, T. Watanabe *et al.*, Sci. Rep. **3**, 1170 (2013).

[23] A. P. L. Robinson, M. Sherlock, and P. A. Norreys, Phys. Rev. Lett. **100**, 025002 (2008).

[24] R. H. H. Scott, C. Beaucourt, H.-P. Schlenvoigt, K. Markey, K. L. Lancaster, C. P. Ridgers, C. M. Brenner, J. Pasley, R. J. Gray, I. O. Musgrave *et al.*, Phys. Rev. Lett. **109**, 015001 (2012).

[25] F. Pérez, A. Debayle, J. Honrubia, M. Koenig, D. Batani, S. D. Baton, F. N. Beg, C. Benedetti, E. Brambrink, S. Chawla *et al.*, Phys. Rev. Lett. **107**, 065004 (2011).

[26] B. Ramakrishna, S. Kar, A. Robinson, D. J. Adams, K. Markey, M. N. Quinn, X. H. Yuan, P. McKenna, K. L. Lancaster, J. S. Green *et al.*, Phys. Rev. Lett. **105**, 135001 (2010).

[27] A. P. L. Robinson, M. H. Key, and M. Tabak, Phys. Rev. Lett. **108**, 125004 (2012).

[28] S. Agostinelli, J. Allison, K. Amako, J. Apostolakis, H. Araujo, P. Arce, M. Asai, D. Axen, S. Banerjee, G. Barrand *et al.*, Nucl. Instrum. Methods Phys. Res. Sect. A Accel. Spectrometers, Detect. Assoc. Equip. **506**, 250 (2003).

[29] T. Sato, K. Niita, N. Matsuda, S. Hashimoto, Y. Iwamoto, S. Noda, T. Ogawa, H. Iwase, H. Nakashima, T. Fukahori *et al.*, J. Nucl. Sci. Technol. **50**, 913 (2013).

[30] S. Atzeni and M. Tabak, Plasma Phys. Controlled Fusion **47**, B769 (2005).

[31] H. Sakagami, T. Johzaki, H. Nagatomo, and K. Mima, Laser Part. Beams **24**, 191 (2006).

[32] C. D. Chen, J. A. King, M. H. Key, K. U. Akli, F. N. Beg, H. Chen, R. R. Freeman, A. Link, A. J. Mackinnon, A. G. MacPhee *et al.*, Rev. Sci. Instrum. **79**, 10E305 (2008).

[33] Z. Zhang, H. Nishimura, T. Namimoto, S. Fujioka, Y. Arikawa, M. Nishikino, T. Kawachi, A. Sagisaka, H. Hosoda, S. Orimo *et al.*, Rev. Sci. Instrum. **83**, 053502 (2012).

[34] J. R. Davies, R. Betti, P. M. Nilson, and A. A. Solodov, Phys. Plasmas **20**, 083118 (2013).

[35] T. Johzaki, Y. Nakao, and K. Mima, Phys. Plasmas **16**, 062706 (2009).

[36] H. Nagatomo, T. Johzaki, T. Nakamura, H. Sakagami, A. Sunahara, and K. Mima, Phys. Plasmas **14**, 056303 (2007).

[37] S. C. Wilks, W. L. Kruer, M. Tabak, and A. B. Langdon, Phys. Rev. Lett. **69**, 1383 (1992).

[38] F. N. Beg, A. R. Bell, A. E. Dangor, C. N. Danson, A. P. Fews, M. E. Glinsky, B. A. Hammel, P. Lee, P. A. Norreys, and M. Tatarakis, Phys. Plasmas **4**, 447 (1997).

[39] T. Tanimoto, H. Habara, R. Kodama, M. Nakatsutsumi, K. A. Tanaka, K. L. Lancaster, J. S. Green, R. H. H. Scott, M. Sherlock, P. A. Norreys *et al.*, Phys. Plasmas **16**, 062703 (2009).

[40] M. G. Haines, M. S. Wei, F. N. Beg, and R. B. Stephens, Phys. Rev. Lett. **102**, 045008 (2009).

[41] Z.-M. Sheng, K. Mima, Y. Sentoku, M. S. Jovanović, T. Taguchi, J. Zhang, and J. Meyer-ter-Vehn, Phys. Rev. Lett. **88**, 055004 (2002).

[42] A. Bourdier, D. Patin, and E. Lefebvre, Laser Part. Beams **25**, 169 (2007).

[43] A. J. Kemp, Y. Sentoku, and M. Tabak, Phys. Rev. E **79**, 066406 (2009).

[44] S. Backus, H. C. Kapteyn, M. M. Murnane, D. M. Gold, H. Nathel, and W. White, Opt. Lett. **18**, 134 (1993).

[45] G. Doumy, F. Quéré, O. Gobert, M. Perdrix, P. Martin, P. Audebert, J. C. Gauthier, J. P. Geindre, and T. Wittmann, Phys. Rev. E **69**, 026402 (2004).